Onconase: An Unusually Stable Protein†

Eugenio Notomista,‡ Francesca Catanzano,§ Giuseppe Graziano,|| Fabrizio Dal Piaz,‡,⊥ Guido Barone,§ Giuseppe D'Alessio,‡ and Alberto Di Donato*,‡

Dipartimento di Chimica Organica e Biologica, Università di Napoli Federico II, Via Mezzocannone 16, 80134 Naples, Italy, Dipartimento di Chimica, Università di Napoli Federico II, Via Mezzocannone, 4-80134 Naples, Italy, Facoltà di Scienze, Università del Sannio Via Port'Arsa, 11-82100 Benevento, Italy, and Centro Internazionale di Servizi di Spettrometria di Massa, Via Pansini, 5. 80131 Naples, Italy

Received February 23, 2000; Revised Manuscript Received May 3, 2000

ABSTRACT: Several members of the RNase A superfamily are endowed with antitumor activity, showing selective cytotoxicity toward tumor cell lines. One of these is onconase, the smallest member of the superfamily, which at present is undergoing phase-III clinical trials as an antitumor drug. Our investigation focused on other interesting features of the enzyme, such as its unusually high denaturation temperature, its low catalytic activity, and its renal toxicity as a drug. We used differential scanning calorimetry, circular dichroism, fluorescence measurements, and limited proteolysis to investigate the molecular determinants of the stability of onconase and of a mutant, (M23L)-ONC, which is catalytically more active than the wild-type enzyme, and fully active as an antitumor agent. The determination of the main thermodynamic parameters of the protein led to the conclusion that onconase is an unusually stable protein. This was confirmed by its resistance to proteolysis. On the basis of this analysis and on a comparative analysis of the (M23L)-ONC variant of the protein, which is less stable and more sensitive to proteolysis, a model was constructed in line with available data. This model supports a satisfactory hypothesis of the molecular basis of onconase stability and low-catalytic activity.

At least four members of the RNase A (bovine pancreatic ribonuclease)[1] superfamily are endowed with antitumor activity and show selective cytotoxicity toward several tumor cell lines: bovine seminal ribonuclease (BS-RNase) from bull semen, onconase (ONC) from oocytes of *Rana pipiens*, and the closely related sialic acid-binding lectins from oocytes of *Rana catesbeiana* and *Rana japonica* (*1*). These proteins have been extensively studied because of their potential as antitumor drugs, and ONC has reached phase-III clinical trials (*2*).

ONC is the smallest member of the RNase A superfamily, with 104 residues as compared to the 124 in the primary structure of RNase A, and shares 30% identity with the RNase A sequence (*3*). Despite the low degree of identity between their primary structures, the three-dimensional structure of ONC (*4*) shows a topology very similar to that of RNase A (Figure 1), with the major differences present in the loop regions and at the C-terminus, where ONC has an additional disulfide bond (Cys87−Cys104), which is found only in frog RNases (*4*, *5*). It should be noted that a strong similarity in three-dimensional structures is a common trait in the superfamily. Thus, the RNases show divergent primary structures (*6*, *7*) as well as a well-preserved tertiary fold marked by a core structure made up of two antiparallel β-sheets and three α-helices.

It has been reported (*8*) that ONC has an unusually high denaturation temperature, which positions ONC among the most thermostable mesophilic proteins found so far. Indeed, if the high T_d measured for ONC is a consequence of its stability, this might well be the cause for both the low catalytic activity of the protein (*9*, *10*) and its renal toxicity (*11*). In fact, if the stability of the protein is based on its intrinsic rigidity, as is the case for most thermophilic proteins (*12*), this could explain both (i) its low activity, and thus, its low flexibility in adapting to the substrate and/or to the transition state, the key event in the catalytic mechanism (*13*), and (ii) its renal toxicity, for the difficulty in clearing the protein, resulting in its high concentration in the kidney, which can lead to renal damage.

To investigate the determinants of the stability of ONC, we studied by differential scanning calorimetry, circular dichroism, and fluorescence measurements the main thermodynamic parameters of the protein and of a mutant,

† This work was supported by grants from the Ministry of University and Research (PRIN/97, SMIP, and PRIN/97, CFSIB), the MURST-CNR Program L. 95/95, and the National Research Council (PF−Biotecnologie).

* To whom correspondence should be addressed. Phone: +39-081-7041 271. Fax: +39-081-552 1217. E-mail: didonato@unina.it.

‡ Dipartimento di Chimica Organica e Biologica, Università di Napoli Federico II.

§ Dipartimento di Chimica, Università di Napoli Federico II.

|| Facoltà di Scienze, Università del Sannio.

⊥ Centro Internazionale di Servizi di Spettrometria di Massa.

[1] BS-RNase, bovine seminal ribonuclease; RNase A, bovine pancreatic ribonuclease A; ONC, Onconase; (M23L)-ONC, mutant of onconase with leucine replacing methionine at position 23; (Q1E)-ONC, mutant of onconase with glutamic acid replacing glutamine at position 1; ES/MS, electrospray mass spectrometry; DSC, differential scanning calorimetry; CD, circular dichroism; ASA, accessible surface area; MES, 2-(*N*-morpholino)ethanesulfonic acid; HEPPSO, *N*-(2-hydroxyethyl)piperazine-*N*′-(2-hydroxypropanesulfonic acid); Tris, tris(hydroxymethyl)aminomethane; PMSF, phenylmethanesulfonyl fluoride; EDTA, ethylenediaminetetraacetic acid; CNBr, cyanogen bromide; DTT, dithiothreitol; TFA, trifluoroacetic acid; GuHCl, guanidinium chloride; RP-HPLC, reverse-phase high-performance liquid chromatography; PDB, Protein Data Bank.

10.1021/bi000415x CCC: $19.00
Published on Web 07/06/2000

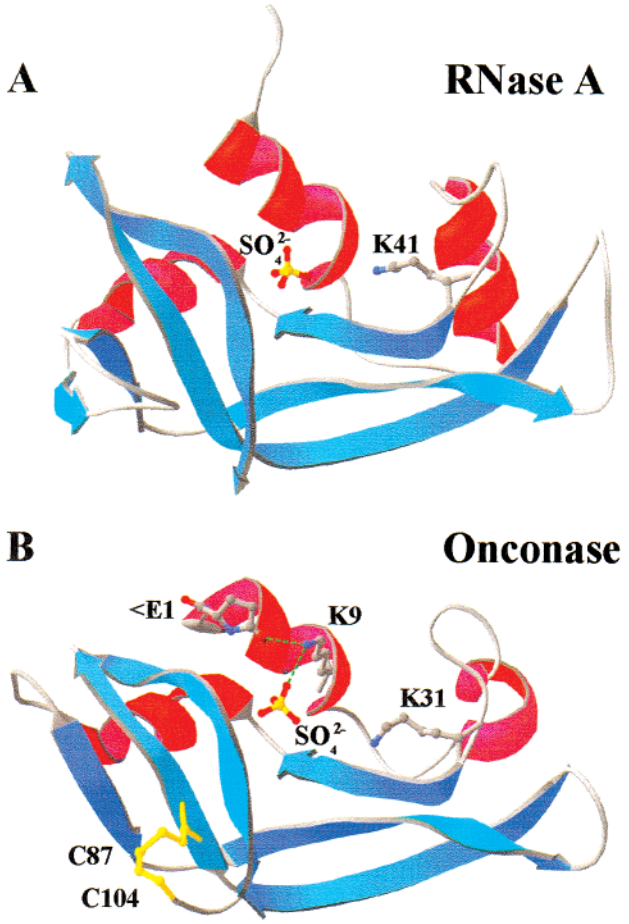

FIGURE 1: (A) Crystal structures of RNase A (A) (PDB accession code: 7RSA) and of ONC (B) (PDB accession code: 1ONC). Helices are colored in red and β-strands are colored in light blue. Sulfate anions and residues of the active sites are colored according to the following code: carbon atoms, gray; nitrogen atoms, blue; oxygen atoms, red; sulfur atoms, yellow. C-terminal disulfide bridge (C87−C104) in ONC is colored in yellow. Green dotted lines indicate hydrogen bonds.

(M23L)-ONC, which is catalytically more active than the wild-type enzyme, and is found to possess a full antitumor activity (*9*, *14*). This mutant was first designed by Boix (*9*) while establishing an expression system for recombinant ONC. Substitution of a methionine by a leucine residue at position 23 was aimed at leaving a single methionine residue at the N-terminus so that CNBr could be used to remove Met(-1) from the recombinant protein in order to produce a mature protein. We also probed ONC and its mutant with proteolytic enzymes and discovered that the introduction at position 23 of a leucine for a methionine destabilizes the protein, lowering its denaturation temperature and increasing its catalytic activity. A hypothesis about the effects of the mutation on the ONC structure was derived on the basis of a structural model of the mutant protein.

MATERIALS AND METHODS

Materials. Plasmid pET22b(+) and *Escherichia coli* strain BL21(DE3) were purchased from AMS Biotechnology. *E. coli* strain JM101 was purchased from Boehringer, and labeled oligonucleotides were purchased from Amersham. The Wizard DNA purification kit for elution of DNA fragments from agarose gel, enzymes, and other reagents for DNA manipulation were purchased from Promega.

General Procedures. Bacterial cultures, plasmid purifications, and transformations were performed according to Sambrook et al. (*15*). Double-stranded DNA was sequenced using the dideoxy method of Sanger et al. (*16*) and carried out using a Sequenase version II kit (Amersham) and deoxynucleotide triphosphates purchased from Pharmacia.

Recombinant Protein Expression and Purification. The cDNA coding for Met(-1)(Q1E)-ONC cloned between the *Nde*1 and *Bam*H1 sites of vector pET11d, kindly provided by Dr. R. J. Youle (National Institute of Neurological Disorders and Stroke, NIH), was subcloned into vector pET22b(+). Oligonucleotide-mediated site-directed mutagenesis, performed according to the process described by Kunkel (*17*), was used to restore the glutamine residue at position 1 and to yield the cDNA coding for recombinant ONC. This cDNA was further mutated to replace the methionine residue at position 23, yielding the coding sequence for mutant (M23L)-ONC. Both proteins were expressed and purified as described (*14*), with an average yield of about 40 mg of protein/liter of bacterial culture. Recombinant ONC and mutant (M23L)-ONC were characterized by N-terminal sequencing, by determination of their molecular weight by ES/MS, and by their catalytic activity on yeast RNA (*18*, *19*).

Scanning Calorimetry. Calorimetric measurements were carried out on a Setaram Micro-DSC apparatus interfaced with a data-translation A/D board for automatic data accumulation. A scan rate of 0.5 K min^{-1} was chosen for the present study. All data analyses were performed using the software described by Catanzano et al. (*20*). The excess heat capacity function $\langle\Delta C_p\rangle$ was obtained after baseline subtraction, assuming that the baseline is given by a linear temperature-dependent extrapolation of the native-state heat capacity (*21*). Calorimetric enthalpy $\Delta_d H(T_d)$ was determined by direct integration of the area under the curve, and the van't Hoff enthalpy was calculated using the formula (*22*)

$$\Delta_d H_{vH}(T_d) = 4RT_d^2[\langle\Delta C_p(T_d)\rangle/\Delta_d H(T_d)] \quad (1)$$

where T_d is the denaturation temperature and corresponds to the maximum of the DSC peak, $\langle\Delta C_p(T_d)\rangle$ is the value of excess molar heat capacity function at T_d, and R is the gas constant. The close correspondence between calorimetric enthalpy $\Delta_d H(T_d)$ and van't Hoff enthalpy $\Delta_d H_{vH}(T_d)$ is a necessary condition in order to define the denaturation process as a two-state transition (*22*, *23*).

The denaturation Gibbs energy change at 25 °C was calculated using the equation

$$\Delta_d G(T) = \Delta_d H(T_d)[1 - (T/T_d)] + \Delta_d C_p[T - T_d - T\ln(T/T_d)] \quad (2)$$

in which $\Delta_d C_p$ is considered temperature-independent.

Buffers were purchased from Sigma and included GlyHCl, acetic acid/sodium acetate, MES, and HEPPSO. The buffer systems used have low protonation enthalpies (*24*), and therefore, their pH values depend little on temperature. Doubly deionized water was used throughout. The pH of all samples was measured before each measurement, at 25 °C, with a Radiometer pH meter (model PHM93). Before DSC measurements, protein solutions were dialyzed against the required buffer at 4 °C for 24 h and were degassed for 5

min. The protein concentration of dialyzed samples was determined spectrophotometrically using $\epsilon_{280} = 10\,400\ M^{-1}\ cm^{-1}$.

GuHCl-Induced Denaturation. Ultrapure GuHCl was purchased from Pierce, and 8 M stock solutions were prepared in water as described (*25*). Stock protein solutions (50-fold their final concentrations) were prepared in 100 mM MES buffer at pH 6.0. Working solutions were prepared in 1.5 mL siliconized Eppendorf tubes using variable amounts of 8 M GuHCl, 10 μL of stock protein solution, and water to a final volume of 500 μL. The pH value of the solutions was kept constant by adding concentrated NaOH. Each sample was mixed by vortexing and incubated for 24 h at 4 °C.

CD measurements were performed with a JASCO J-710 spectropolarimeter at a protein concentration of 1 mg mL^{-1} in 100 mM MES buffer, pH 6.0, containing GuHCl. Molar ellipticity at 222 nm is reported as mean residue molar ellipticity, $[\theta]_{222}$ in deg cm^2 $dmol^{-1}$, calculated from the equation: $[\theta] = \{[\theta]_{obs}(mrw)\}/(10lC)$, where $[\theta]_{obs}$ is the ellipticity measured in degrees, mrw is the mean residue molecular mass (110 Da), C is the protein concentration in grams per milliliter, and l is the optical path length of the cell in centimeters. The instrument was equipped with thermostated cell holders, and temperature was kept constant at 25 °C using a circulating water bath.

Fluorescence emission spectra were recorded with a Jasco FP777 spectrofluorimeter at a protein concentration of 0.05 mg mL^{-1} in 100 mM MES buffer, pH 6.0, containing GuHCl. The excitation wavelength was set at 280 nm to include the tyrosine contribution to the overall fluorescence emission because ONC possesses only one tryptophan residue at position 3. Experiments were performed at 25 °C using a sealed quartz cell which had a 1-cm path length, a 5-nm slit width, and corrected for background signal. Only the shift in fluorescence maximum wavelength was used to monitor protein denaturation.

The two-state N ⇔ D transition model, whose equilibrium constant K_d is related to the standard Gibbs energy change by the thermodynamic equation $\Delta_d G = -RT \ln K_d$, was used to analyze the GuHCl-induced denaturation of ONC. The linear extrapolation model (LEM) was used, as modified by Santoro and Bolen (*26*). A linear variation of $\Delta_d G$ was assumed, with the denaturant concentration (C_{GuHCl}), according to the equation

$$\Delta_d G = \Delta_d G_{H_2O} - mC_{GuHCl} \quad (3)$$

where $\Delta_d G_{H_2O}$ is the value of $\Delta_d G$ in the absence of GuHCl and m is a measure of the dependence of $\Delta_d G$ on GuHCl concentration. Furthermore, $\Delta_d G_{H_2O} = m(C_{GuHCl})_{1/2}$, where $(C_{GuHCl})_{1/2}$ is a measure of the midpoint of the denaturation region. Also, the spectroscopic signals of native (Y_N) and denatured (Y_D) states are assumed to vary linearly with GuHCl concentration, following the equation $Y_i = a_i + b_i C_{GuHCl}$, with b_i being the corresponding slope. Under these assumptions, the observed spectroscopic signal is given by

$$Y = \{Y_N + Y_D \exp[-(\Delta_d G_{H_2O} - mC_{GuHCl})/RT]\}/\{1 + \exp[-(\Delta_d G_{H_2O} - mC_{GuHCl})/RT]\} \quad (4)$$

A nonlinear least-squares regression was carried out to estimate the unknown parameters associated with the conformational transition according to the minimum χ^2 value. The nonlinear regression used the Levenberg−Marquardt algorithm as implemented in the Optimization Toolbox of MATLAB.

Proteolysis Experiments. ONC and (M23L)-ONC at 0.8 mg mL^{-1} were treated with pepsin at a ratio of 1/10, pepsin/ribonuclease (w/w), in 50 mM GlyHCl at pH 2.4 and 37 °C. Aliquots of the reaction mixture were withdrawn at suitable time intervals, and the reaction was stopped by raising the pH of the solution to 8.0 by the addition of concentrated Tris base. Then 2-mercaptoethanol and SDS were added to final concentrations of 20 mM and 0.1% (w/v), respectively.

Proteins (0.8 mg mL^{-1}) were treated at 37 °C with chymotrypsin at a ratio of 1/50, chymotrypsin/ribonuclease (w/w), in 100 mM Tris-HCl, pH 8.0, containing 10 mM $CaCl_2$. Aliquots of the reaction mixture were withdrawn at suitable time intervals, and the reaction was stopped by the addition of PMSF to a final concentration of 0.5 mM. EDTA, 2-mercaptoethanol, and SDS were added at final concentrations of 15 mM, 20 mM, and 0.1% (w/v), respectively. After 5 min at 100 °C, the samples were analyzed by SDS−PAGE, and Coomassie stained bands were quantified by densitometry.

For the determination of the masses of the proteolytic fragments released by the proteases, peptide mixtures were first reduced with DTT at a ratio of 10/1, DTT/protein total $^1/_2$ cystines (mol/mol), in 0.5 M GuHCl for 2 h, and carboxyamidomethylated using iodoacetamide at a ratio of 20/1, iodoacetamide/DTT (mol/mol), for 30 min at pH 8.4. The peptide mixtures were analyzed by RP-HPLC on a Phenomenex Jupiter C18 reverse-phase column (250 × 2.1 mm, 100-Å pore size) and were eluted at 0.2 mL min^{-1} using a linear gradient in a two-solvent system. Solvent A was 0.1% TFA in water; solvent B was acetonitrile containing 0.1% TFA. The gradient was constructed by increasing the concentration of solvent B from 20 to 60% in 50 min. Individual fractions were collected and identified by ES/MS.

Mass Spectrometry. Protein samples or proteolytic fragments were analyzed at CEINGE Biotecnologie Avanzate (Naples, Italy) by ES/MS using either a BIO-Q triple-quadrupole mass spectrometer (Micromass, Manchester, U.K.) or an API-100 single-quadrupole instrument (Perkin-Elmer, Norwalk, CT). Samples were directly injected into the ion source via a loop injection at a flow rate of 5 μL min^{-1}. Data were acquired and elaborated using either the MASS-LINX (Micromass, Manchester, U.K.) or the Biomultiviewer (Perkin-Elmer, Norwalk, CT) program. Mass calibration was performed by means of the multiply-charged ions from a separate injection of horse heart myoglobin (average molecular mass 16 951.5 Da). All masses are reported as average mass.

Protein Modeling and Flexibility Predictions. Protein modeling was carried out using the automated comparative-protein server freely available at http://www.expasy.ch/swissmod/SWISS-MODEL.html (*27*). Models were energy-minimized using Gromos96 and were examined using the program Swiss-PDB−Viewer (*28*).

Protein flexibility predictions were carried out using the FLEXPRO program based on the method developed by

Table 1: Thermodynamic Parameters from DSC Measurements of Temperature-Induced Denaturation of ONC and (M23L)-ONC at Different pHs

protein	pH	T_d[a] (°C)	$\Delta_dH(T_d)$[a] (kJ mol^{-1})	$\Delta_dS(T_d)$[a] (kJ K^{-1} mol^{-1})	Δ_dC_p[a] (kJ K^{-1} mol^{-1})	*CU*	Δ_dG(25 °C)[b] (kJ mol^{-1})
ONC	2.0	69.5	425	1.24	6.2	0.97	37.0
	2.5	72.6	440	1.27	5.5	1.01	39.9
	3.0	76.5	470	1.34	6.0	1.02	45.2
	3.5	81.6	500	1.41	5.7	1.01	51.1
	4.0	86.8	525	1.46	5.2	0.99	56.3
	5.0	88.3	540	1.49	6.4	0.98	59.1
	6.0	88.7	540	1.49	5.5	1.01	59.2
	7.0	87.8	530	1.47	6.0	1.03	57.3
	8.0	85.4	515	1.44	5.8	0.97	54.3
(M23L)-ONC	2.0	62.2	355	1.06	5.2	0.96	26.5
	2.5	65.8	380	1.12	6.3	1.04	30.3
	3.0	68.9	400	1.17	5.8	1.01	33.6
	3.5	74.7	430	1.24	6.2	1.03	39.0
	4.0	80.7	470	1.33	5.6	0.98	46.2
	5.0	82.3	480	1.35	6.0	0.98	48.0
	6.0	82.8	480	1.35	5.4	1.02	48.1
	7.0	82.0	480	1.35	6.1	0.97	48.0
	8.0	79.1	460	1.31	5.7	1.01	44.3

[a] Each value is the mean value of four measurements. Error for T_d does not exceed 0.2 °C. Errors for $\Delta_dH(T_d)$ and Δ_dC_p are 5% and 10%, respectively. CU is the cooperative unit, i.e., the ratio of the calorimetric to van't Hoff enthalpy at the denaturation temperature. [b] Values of Δ_dG(25 °C) have been calculated as described in the text, using the parameters determined by DSC measurements.

Karplus and Schulz (*29*), which allows prediction of the local flexibility of a polypeptide chain by using crystallographic B-factors from a large set of protein structures. Predictions were also made using the program ProtScale, available at http://www.expasy.ch/cgi-bin/protscale.pl, which uses flexibility indexes defined by Bhaskaran and Ponnuswamy (*30*, *31*).

Other Methods. Protein sequence determinations were performed on an Applied Biosystems (Foster City, CA) sequenator (model 473A) which was connected on-line with a high-performance liquid chromatography apparatus for identification of phenylthiohydantoins. RNase activity on yeast RNA was assayed using the method of Kunitz (*18*) or by the precipitation assay (*19*). SDS−PAGE was carried out according to Schagger (*32*).

RESULTS

Temperature-Induced Denaturation. To investigate the thermal stability of ONC and (M23L)-ONC, DSC measurements were performed in the protein concentration range 1.4−3.0 mg mL^{-1}, in 100 mM buffer, and in the pH range 2.0−8.0. The results are listed in Table 1. Representative DSC curves at pH 6.0 for both wild-type and the mutant are shown in Figure 2. The temperature-induced denaturation is well-represented by the two-state N ⇔ D transition model, as indicated by the closeness to one of the cooperative units, defined as the calorimetric-to-van't Hoff enthalpy ratio, $CU \equiv \Delta_dH(T_d)/\Delta_dH_{vH}(T_d)$. All transitions were reversible, as judged by the reheating criterion, and were not influenced by protein concentration, thus further confirming the two-state N ⇔ D model.

The values of both T_d and $\Delta_dH(T_d)$, measured for ONC, progressively increase from 69.5 °C and 425 kJ mol^{-1} at pH 2.0 to 88.7 °C and 540 kJ mol^{-1} at pH 6.0 (Table 1). With further increasing pH, thermal stability slightly decreases: T_d = 85.4 °C and $\Delta_dH(T_d)$ = 515 kJ mol^{-1} at pH 8.0.

The values of the denaturation temperature for (M23L)-ONC show a similar trend, even though at all pH values

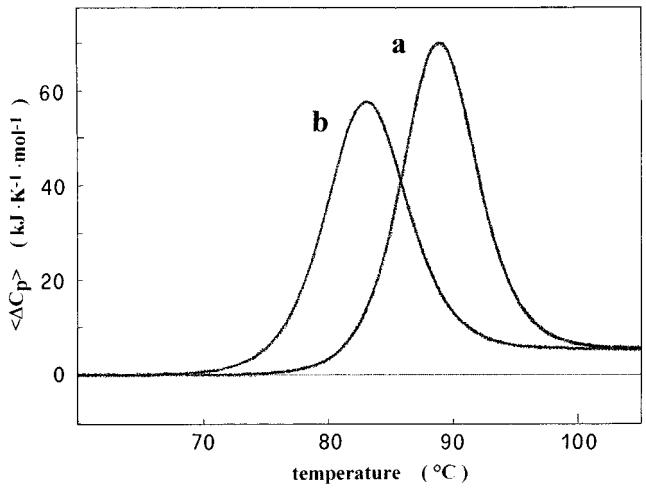

FIGURE 2: DSC profiles, at pH 6.0 in 100 mM MES buffer, of ONC (a) and (M23L)-ONC (b).

they are lower than those measured for ONC by about 6 °C. At pH 6.0, where the two proteins show the maximal stability, a T_d value of 82.8 °C and a $\Delta_dH(T_d)$ value of 480 kJ mol^{-1} were measured for (M23L)-ONC, lower than those measured for parent ONC (see above). The finding that the pH dependence of the thermal stability of (M23L)-ONC parallels that of the parent enzyme is not surprising because the single amino acid substitution M23L does not alter the content of ionizable groups in the protein.

Linear regression of $\Delta_dH(T_d)$ versus T_d plots gave for both proteins $\Delta_dC_p = 6.0 \pm 0.5$ kJ K^{-1}mol^{-1} ($r = 0.99$). This value agrees with the estimate of 5.6 kJ K^{-1} mol^{-1}, which is obtained by means of an empirical relationship which is based on the additivity of polar and nonpolar group contributions, weighted on the basis of their burial in the protein interior (*33*).

The values of denaturation Gibbs energy change Δ_dG at 25 °C, calculated using eq 2, are reported in the last column of Table 1. They confirm that the two proteins have a maximal thermodynamic stability around pH 6.0 and that

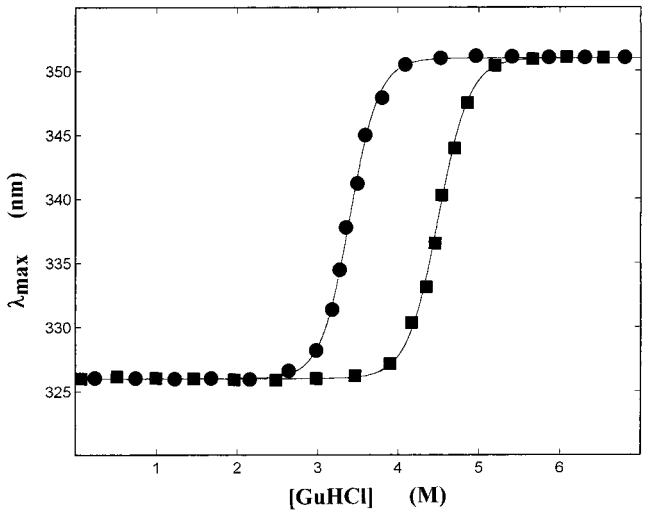

FIGURE 3: GuHCl denaturation curves determined by monitoring the shift in fluorescence maximum wavelength at 25 °C, pH 6.0, and 100 mM MES buffer. The circle is ONC; the square, (M23L)-ONC. Solid lines are the results of the nonlinear least-squares regressions of the experimental data.

(M23L)-ONC is less stable than ONC. In fact, the estimates of $\Delta_d G$(25 °C) for (M23L)-ONC are about 10 kJ mol^{-1} lower than those of the parent protein at all pH values.

For the comparison of the denaturation enthalpy and entropy changes of the two proteins at the same temperature (*34*), we selected the denaturation temperature of (M23L)-ONC at pH 6.0, 82.8 °C, and calculated $\Delta_d H$ and $\Delta_d S$, assuming a constant $\Delta_d C_p$ value equal to 6.0 kJ K^{-1} mol^{-1}. Values of $\Delta_d H$(82.8 °C) = 505 kJ mol^{-1} and $\Delta_d S$(82.8 °C) = 1.39 kJ K^{-1} mol^{-1} were obtained for ONC. These values indicate that the destabilization caused by the replacement of leucine for methionine is due to enthalpic factors, partially counterbalanced by entropic ones.

GuHCl-Induced Denaturation at pH 6.0. To further compare the stability of ONC with that of (M23L)-ONC, the shift in fluorescence maximum wavelength upon excitation at 280 nm and the molar ellipticity at 222 nm were used to monitor the GuHCl-induced denaturation of the proteins. The experiments were carried out at 25 °C in 100 mM MES, pH 6.0. Denaturation proved to be reversible for both proteins and was analyzed by the two-state N ⇔ D model, as described in Materials and Methods. The GuHCl-induced denaturation curves are shown in Figure 3, and the values of parameters m, $\Delta_d G_{H_2O}$, and $(C_{GuHCl})_{1/2}$, derived from nonlinear regressions of the experimental data, are listed in Table 2. The experimental data indicate that the single substitution M23L causes a significant decrease in stability. The value of $(C_{GuHCl})_{1/2}$ is reduced from 4.5 M for ONC to 3.4 M for (M23L)-ONC. Moreover, the value of $\Delta_d G_{H_2O}$ is about 58.0 kJ mol^{-1} for ONC and about 47.0 kJ mol^{-1} for (M23L)-ONC. It should also be noted that these values agree, within the experimental error, with those calculated at 25 °C using eq 2 and the parameters determined by DSC measurements (see last column of Table 1). The satisfactory agreement must be underlined between the $\Delta_d G$ values calculated using two different experimental procedures, based on different equations.

Moreover, it should be noted that the values obtained for m and $\Delta_d C_p$ are very similar for ONC and (M23L)-ONC (see Tables 1 and 2). Because it has been clearly demonstrated that both parameters are proportional to the difference in solvent-accessible surface area (ΔASA) between the denatured and native states (*35*), we can confidently conclude that there should be no significant difference in ΔASA between the two proteins.

Table 2: Thermodynamic Parameters of the GuHCl-Induced Denaturation of ONC and (M23L)-ONC at 25 °C, pH 6.0[a]

protein	$(C_{GuHCl})_{1/2}$[d] (M)	m[e] (kJ mol^{-1}M^{-1})	$\Delta_d G_{H_2O}$[e] (kJ mol^{-1})
ONC[b]	4.5	12.9 ± 0.8	58.0 ± 2.5
ONC[c]	4.5	13.1 ± 0.7	59.0± 2.2
(M23L)-ONC[b]	3.4	13.8 ± 1.0	47.0 ± 2.8
(M23L)-ONC[c]	3.4	13.6 ± 0.8	46.2 ± 2.0

[a] The reported values are the results of nonlinear least-squares regressions for the plots of the shift in the fluorescence maximum wavelength or of the molar ellipticity at 222 nm as a function of GuHCl concentration. [b] Values obtained following the shift in the fluorescence maximum wavelength. [c] Values obtained following the molar ellipticity at 222 nm. [d] $(C_{GuHCl})_{1/2} = [\Delta_d G_{H_2O}/m]$ is the midpoint of the GuHCl denaturation curve. [e] Errors are the standard deviations of nonlinear regressions.

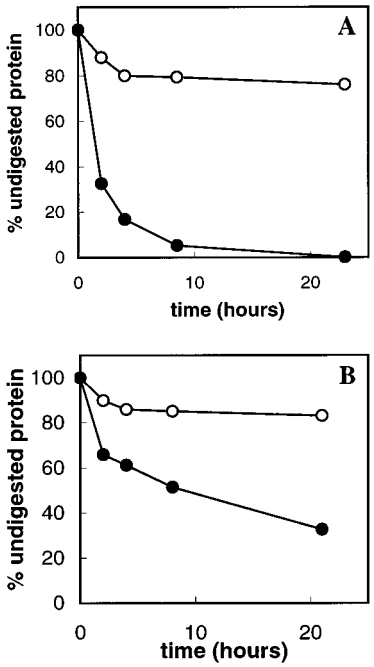

FIGURE 4: Densitometric curves of proteolytic digestion of ONC (○), (M23L)-ONC (●) by pepsin (A) and chymotrypsin (B). The curves were obtained as described in the Materials and Methods section.

Proteolysis Experiments. To probe the structural rigidity of ONC and (M23L)-ONC, both proteins were subjected to limited proteolysis by using pepsin and chymotrypsin as conformational probes. Pepsin and chymotrypsin were chosen for their broad specificity (*36*) so that the sites of proteolytic cleavage would mainly depend on the accessibility of the substrate rather than on its primary structure.

ONC proved to be particularly resistant to both pepsin and chymotrypsin. Only about 20% of ONC was digested in 23 h (Figure 4A,B). Conversely, (M23L)-ONC was degraded much more effectively and was almost completely digested in about 20 h (Figure 4A,B).

To identify the proteolytic cleavage sites, ONC and (M23L)-ONC were digested with either chymotrypsin or

Table 3. Identification of the Peptides Released by Chymotrypsin or Pepsin from ONC and (M23L)-ONC

protease	protein	determined mass (Da)[a,b]	peptide	theoretical mass (Da)[a]
chymotrypsin	ONC	8878.4	His29−Cys104	8878.3
	(M23L)-ONC	8877.4		
	ONC	1890.8	Leu4−Arg15	1891.5
	(M23L)-ONC	1891.3		
	ONC	1549.0	Asp16−Phe28	1549.3
	(M23L)-ONC	1524.1		1524.4
pepsin	ONC	5093.3	His29−Ser72	5093.9
	(M23L)-ONC	5094.1		
	ONC	3746.0	Arg73−Cys104	3745.4
	(M23L)-ONC	3745.2		
	ONC	4054.8	His29−Phe63	4054.0
	(M23L)-ONC	4054.3		
	ONC	1057.6	Tyr64−Ser72	1057.9
	(M23L)-ONC	1057.5		

[a] Mass values of peptides carboxyamidomethylated at cysteine residues (see Materials and Methods). [b] Errors were always lower than 1 Da.

pepsin for different time intervals (10 min to 21 h). After digestion, the proteins were reduced and carboxyamidomethylated. The resulting peptides were separated by RP-HPLC and identified on the basis of their molecular weights as determined by ES/MS measurements (Table 3).

At all time intervals, a similar peptide pattern was obtained for each protein. There were few relevant fragments, except others which were detected in amounts too low to be further analyzed (data not shown).

In chymotryptic digests of both ONC and (M23L)-ONC, only one large peptide (8878.4 Da), corresponding to fragment 29−104, and a few short peptides were found (Table 3) in addition to the undigested proteins. Interestingly, for both proteins, the amount of fragment 29−104 was rather low and did not increase with digestion time. The complementary fragment, peptide 1−28, was never detected, even at short digestion times. Instead, fragments derived from further digestion of peptide 1−28, that is, peptides 4−15 and 16−28, were found, indicating that the peptide bonds between Trp3 and Leu4 and between Arg15 and Asp16 were readily susceptible to proteolytic attack. It should be reminded that cleavages at arginine residues are rather unusual for chymotrypsin on protein substrates (*36*). Thus, the hydrolysis of the peptide bond between Arg15 and Asp16 is likely a subdigestion site, which is made available to chymotrypsin in the peptide substrate produced by the primary digestion events.

The limited proteolysis pattern produced by chymotrypsin would indicate that the peptide bond between Phe28 and His29, and/or the bond between Trp3 and Leu4 are possibly the first cleavage sites of the polypeptide chains. Moreover, although the chymotryptic digestion pattern was identical for both ONC and (M23L)-ONC, the rate of proteolysis was higher for the mutant protein with respect to native ONC (see Figure 4B). Thus, it can be concluded that the peptide bonds Phe28-His29 and/or Trp3-Leu4 are more accessible in the mutant than in wild-type ONC.

In the pepsin digests of both proteins, the following fragments were found: peptides 29−63, 29−72, 73−104, and 64−72 (see Table 3), derived from cleavages at peptide bonds Phe28−His29, Phe63−Tyr64, and Ser72−Arg73. These results indicate that the peptide bonds Phe28−His29 and Ser72−Arg73 may be the first sites to be cleaved by pepsin in both ONC and (M23L)-ONC. Also, in the peptic digest the fragment 1−28 was not detected, even at short digestion times. As in the case of chymotrypsin, the digestion pattern was identical for ONC and (M23L)-ONC, but the rate of proteolysis was markedly different, as shown in Figure 4A. It is worth noting that the peptide bond Phe28−His29, which follows the second α-helix (see Figure 1) is cleaved by both pepsin and chymotrypsin. This finding is not surprising, because it is well-known that the loop connecting the second helix to the first β-strand in ribonucleases is recognized by several proteases (*37*, *38*).

DISCUSSION

The data reported in this paper show that ONC is an exceptionally stable protein. DSC data unequivocally indicate that ONC has a high thermal stability: its denaturation temperature is close to 90 °C around pH 6.0 and is close to 70 °C at pH 2.0. The stability of the protein is also evidenced by the value of its stabilization Gibbs energy. For a large number of globular proteins, both monomeric and oligomeric, the stabilization Gibbs energy values at 25 °C, when normalized per residue, are in the range 200−600 J mol^{-1} (*39*, *40*). These values are largely below the random thermal energy at room temperature (i.e., 2500 J mol residue^{-1} at 25 °C), and indicate that the stability of the native structure is marginal and must involve cooperativity (*41*). When the stabilization Gibbs energy at 25 °C normalized per residue is calculated for ONC using the $\Delta_d G$(25 °C) values at pH 6.0 reported in Table 2, a value of about 560 J mol res^{-1} is obtained, which is positioned at the upper limit of the values reported for globular proteins.

The stability of ONC is confirmed by limited proteolysis studies. It has been established that amino acid residues located within exposed and flexible regions of a protein can be recognized by proteases under controlled conditions, leading to a conformational fingerprint of the protein in solution (*42*). The resistance of wild-type ONC to enzymatic cleavage (Figure 4) is indirect evidence that the protein is rather rigid in solution, suggesting that its thermal stability is due to the compactness of its tertiary structure.

The obvious standard for any comparison of ONC conformational stability is the prototype of the pancreatic-type ribonuclease family, RNase A. It has been determined that T_d = 62.4 °C for RNase A at pH 6.0 (*43*), whereas under identical conditions, a T_d value of 88.7 °C has been determined for ONC. The large increase in T_d emphasizes the extra stability of ONC with respect to pancreatic RNase A.

ONC is 20 residues shorter than RNase A and shares only 30% identity with the bovine enzyme. Despite these differences, however, the two proteins show a very similar tertiary fold, with a root-mean-square deviation for backbone atoms of only 1.07 Å. Indeed, deletions are all positioned in the loops and at the N-terminus (Figure 1). One of these deletions removes the residues corresponding to the second β-strand of RNase A and most of the following loop, but it does not alter the global fold because the β-sheet formation is not prevented, as the deleted β-strand occurs at one of its borders (Figure 1). Another interesting deletion, five residues long, is in the loop connecting the first helix to the second one.

To cover the distance between the helices, two residues which are at the beginning of the second α-helix in RNase A (i.e., Asn24 and Tyr25) are replaced by Val17 and Asp18, which are not part of the helix and which adopt a more extended conformation. All of the loops of ONC seem to be reduced to the minimum length necessary to preserve the tertiary fold. Moreover, additional stabilizing factors are at the N-terminus, which is blocked by cyclization into pyroglutamate, and at the C-terminus, with a disulfide bond between the C-terminal Cys104 and Cys87. It is conceivable, then, that this compactness contributes to ONC resistance to denaturants and proteases and to thermal stability.

The variant (M23L)-ONC, which contains a single point mutation (i.e., the replacement of methionine by leucine at position 23), although a very stable protein enzymatically and biologically fully active (*14*), is markedly less stable than the parent protein. Its denaturation temperature (see Table 1) is about 6 °C lower than that of the wild-type protein at all pH values, and its stabilization Gibbs energy at 25 °C and pH 6.0, normalized per residue, is 450 J mol, 110 J mol less than that of ONC. A similar picture is derived from the experiments of GuHCl-induced denaturation (Figure 3 and Table 2). The values obtained for $(C_{GuHCl})_{1/2}$ and for $\Delta_d G_{H_2O}$ confirm the lower stability of (M23L)-ONC with respect to ONC.

Also, the results of limited proteolysis experiments confirm the destabilizing effect of the introduction of a leucine at position 23 of the ONC polypeptide chain. In fact, the (M23L)-ONC is cleaved by pepsin and chymotrypsin under conditions in which the ONC proves to be largely resistant (Figure 4).

These results raise the intriguing question of the molecular basis of the reduced stability of the ONC variant in which a single residue was substituted. Methionine 23 is the last residue of the second helix of ONC spanning from Cys19 to Met23, and it is packed against the first of the two β-sheets which model the characteristic V-shaped motif of the ribonuclease fold (*4*). Molecular modeling indicates that the replacement of the methionine residue at position 23 by a leucine residue should leave a small cavity between the second α-helix and the first β-sheet. This may weaken the packing of the helix on the β-sheet and could provide the basis for the enthalpic destabilization of (M23L)-ONC with respect to ONC.

Moreover, the helix where methionine 23 is located precedes the loop which contains the peptide bond Phe28−His29, which is readily cleaved both by chymotrypsin and pepsin. Our data suggest that this peptide bond is the primary digestion site in both ONC and (M23L)-ONC. In fact, at least in the case of chymotryptic cleavage, in addition to peptides 29−104 and 4−15, peptide 16−28 was also found among the released peptides. The presence of the latter peptide indicates that the bond 23−24 is not cleaved by the proteolytic enzyme, despite the presence of either potentially recognized residues, methionine in the wild-type enzyme or leucine in the mutant protein. Thus, residue 23 (either methionine or leucine) is not a chymotrypsin cleavage site. Inspection of the region surrounding residue Phe28, the residue recognized by chymotrypsin in the cleavage of ONC and (M23L)-ONC, reveals that this is in a pocket defined by the side chains of Lys9, Ile22, Met23, Leu27, and Lys31. Hence, leucine at position 23, which may assume a more compact conformation than that of the methionine residue, could generate a weaker binding of Phe28 to the pocket, thus improving the overall mobility of the loop 24−31 and, therefore, its accessibility to proteases. This is also reinforced by protein flexibility predictions carried out as described in Materials and Methods, which indicate a higher flexibility of the mutant polypeptide chain at the Leu23.

As for the increase in catalytic activity of (M23L)-ONC (*14*), it should be noted that the 24−31 loop also includes Lys31, a residue which plays a crucial role in the catalytic mechanism and corresponds to Lys41 in RNase A (*44*). However, the X-ray structures of the two proteins (*4, 45*), show that Lys31 in ONC is at a distance of 5.4 Å from the sulfate ion at the active site, whereas in RNase A, the distance of Lys41 is 4.8 Å. Since Lys31 in ONC should play the same role as Lys41 in RNase A, a conformational rearrangement would be needed for its optimal catalytic function. We can surmise that the substitution of leucine for methionine at position 23, improving the mobility of the loop 24−31, can facilitate the movement of the Lys31 side chain toward the active site. This possibility is supported by modeling studies. These predict that in (M23L)-ONC, a conformation is allowed for Lys31 side chain which is about 1 Å closer to the active-site sulfate ion with respect to the corresponding distance in ONC. This would explain the increased enzymatic activity of (M23L)-ONC (*14*).

As for the biological significance of the unusual stability of ONC, present in large amounts in oocyte granules where it might have a defensive role against predators of eggs, the biologically relevant consequence of its unusual stability could be its resistance to chemical stresses as well as to the digestive proteases of predators.

It is worth noting that phase-I and -II clinical trials have shown that ONC is degraded slowly in humans, and toxicity is mainly renal, manifested as proteinuria and decreased creatinine clearance (*11*). The high stability of ONC might be related to its biological resistance and could lead to high concentration of the toxin in the kidney and, hence, to renal damage. The results previously reported on (M23L)-ONC, however, show that a partial destabilization of ONC improves its catalytic activity without loss of its antitumor action (*9, 14*). Thus, our data suggest a path toward an improved antitumor agent: a less stable ONC with an intact antitumor activity but decreased toxicity.

ACKNOWLEDGMENT

The authors are indebted to Dr. Richard J. Youle for having kindly provided the cDNA coding for Met(-1)(Q1E, M23L)-ONC and to Dr. Antimo Di Maro for the determination of the N-terminal sequence of the proteins. The authors also thank Dr. Lelio Mazzarella, Department of Chemistry, University of Naples Federico II, for helpful discussions on the structure of ONC.

REFERENCES

1. Youle, R. J., and D'Alessio, G. (1997) in *Ribonucleases. Structures and Function* (D'Alessio, G., and Riordan, J. F., Eds.) pp 491−514, Academic Press, San Diego.
2. Juan, G., Ardelt, B., Li, X., Mikulski, S. M., Shogen, K., Ardelt, W., Mittelman, A., and Darzynkiewicz, Z. (1998) *Leukemia 12*, 1241−8.

3. Ardelt, W., Mikulski, S. M., and Shogen, K. (1991) *J. Biol. Chem. 266*, 245−51.
4. Mosimann, S. C., Ardelt, W., and James, M. N. (1994) *J. Mol. Biol. 236*, 1141−53.
5. Chang, C. F., Chen, C., Chen, Y. C., Hom, K., Huang, R. F., and Huang, T. H. (1998) *J. Mol. Biol. 283*, 231−44.
6. Beintema, J. J., Schuller, C., Irie, M., and Carsana, A. (1988) *Prog. Biophys. Mol. Biol. 151*, 165−92.
7. Beintema, J. J., Breukelman, H. J., Carsana, A., and Furia, A. (1997) in *Ribonucleases. Structures and Function* (D'Alessio, G., and Riordan, J. F., Eds.) pp 245−69, Academic Press, San Diego, CA.
8. Leland, P. A., Schultz, L. W., Kim, B. M., and Raines, R. T. (1998) *Proc. Natl. Acad. Sci. U.S.A. 95*, 10407−12.
9. Boix, E., Wu, Y., Vasandani, V. M., Saxena, S. K., Ardelt, W., Ladner, J., and Youle, R. J. (1996) *J. Mol. Biol. 257*, 992−1007.
10. Newton, D. L., Boque, L., Wlodawer, A., Huang, C. Y., and Rybak, S. M. (1998) *Biochemistry 37*, 5173−83.
11. Vasandani, V. M., Wu, Y. N., Mikulski, S. M., Youle, R. J., and Sung, C. (1996) *Cancer Res. 56*, 4180−6.
12. Fontana, A., De Filippis, V., Polverino de Laureto, P., Scaramella, E., and Zambonin, M. (1998) in *Stability and Stabilization of Biocatalysts* (Ballestreros, A., Plou, F. J., Iborra, J. L., and Halling, P. J., Eds.) pp 277−94, Elsevier, Amsterdam.
13. Fersht, A. (1977) *Enzyme Structure and Mechanism*, 2nd ed., W. H. Freeman, New York.
14. Notomista, E., Cafaro, V., Fusiello, R., Bracale, A., D'Alessio, G., and Di Donato, A. (1999) *FEBS Lett. 463*, 211−5.
15. Sambrook, J., Fritsch, E. F., and Maniatis, T. (1989) *Molecular Cloning. A Laboratory Manual*, 2nd ed., Cold Spring Harbor Laboratory Press, Cold Spring Harbor, NY.
16. Sanger, F., Nicklen, S., and Coulson, A. R. (1977) *Proc. Natl. Acad. Sci. U.S.A. 76*, 5653−67.
17. Kunkel, T. A. (1987) *Proc. Natl. Acad. Sci. U.S.A. 82*, 488−92.
18. Kunitz, M. (1946) *J. Biol. Chem. 164*, 563−8.
19. Blackburn, P., Wilson, G., and Moore, S. (1977) *J. Biol. Chem. 252*, 5904−10.
20. Catanzano, F., Giancola, C., Graziano, G., and Barone, G. (1996) *Biochemistry 35*, 13378−85.
21. Freire, E. (1994) *Methods Enzymol. 240*, 502−30.
22. Privalov, P. L. (1979) *Adv. Protein Chem. 33*, 167−241.
23. Zhou, Y., Hall, C. K., and Karplus, M. (1999) *Protein Sci. 8*, 1064−74.
24. Izatt, R. M., and Christensen, J. J. (1976) in *The CRC Handbook of Biochemistry and Molecular Biology, Physical and Chemical Data* (Fasman, G. D., Ed.) pp 151−269, CRC Press, Boca Raton, FL.
25. Pace, N. C. (1986) *Methods Enzymol. 131*, 266−80.
26. Santoro, M. M., and Bolen, W. (1988) *Biochemistry 27*, 8063−8.
27. Peitsch, M. C. (1996) *Biochem. Soc. Trans. 24*, 274−9.
28. Peitsch, M. C., and Guex, N. (1997) *Electrophoresis 18*, 2714−23.
29. Karplus, P. A., and Schulz, G. E. (1989) *J. Mol. Biol. 210*, 163−80.
30. Ponnuswamy, P. K., and Bhaskaran, R. (1984) *Int. J. Pept. Protein Res. 24*, 168−79.
31. Bhaskaran, R., Prabhakaran, M., Jayaraman, G., Yu, C., and Ponnuswamy, P. K. (1996) *J. Biomol. Struct. Dyn. 13*, 627−39.
32. Schagger, H., and von Jagow, G. (1987) *Anal. Biochem. 166*, 368−79.
33. Graziano, G., Catanzano, F., and Barone, G. (1998) *Thermochim. Acta 321*, 23−31.
34. Catanzano, F., Graziano, G., Cafaro, V., D'Alessio, G., Di Donato, A., and Barone, G. (1997) *Biochemistry 36*, 14403−8.
35. Myers, J. K., Pace, N. C., and Scholtz, J. M. (1995) *Protein Sci. 4*, 2138−48.
36. Beynon, R. J., and Bond, J. S. (1989) in *The Practical Approach Series* (Rickwood, D., and Hames, B. D., Eds.) IRL Press, Oxford, New York, and Tokyo.
37. Arnold, U., Rucknagel, K. P., Shierhorn, A., and Hulbrich-Hofmann, R. (1996) *Eur. J. Biochem. 237*, 862−9.
38. Polverino de Laureto, P., Scaramella, E., De Filippis, V., Bruix, M., Rico, M., and Fontana, A. (1997) *Protein Sci. 6*, 860−72.
39. Makhatadze, G. I., and Privalov, P. L. (1995) *Adv. Protein Chem. 47*, 307−425.
40. Pace, C. N. (1990) *Trends Biochem. Sci. 15*, 147.
41. Jaenicke, R. (1991) *Eur. J. Biochem. 202*, 715−28.
42. Fontana, A., Polverino de Laureto, P., De Filippis, V., Scaramella, E., and Zambonin, M. (1997) *Folding Des. 2* (2 R), 17−26.
43. Catanzano, F., Graziano, G., Capasso, S., and Barone, G. (1997) *Protein Sci. 6*, 1682−93.
44. Richards, F. M., and Wyckoff, H. W. (1971) in *The Enzymes*, pp 647−807, Academic Press, New York.
45. Wlodawer, A., and Sjolin, L. (1983) *Biochemistry 22*, 2720−8.

BI000415X